Strong electron correlation in UO2 : A photoelectron spectroscopy and relativistic quantum chemistry study

Wei-Li Li, Jing Su, Tian Jian, Gary V. Lopez, Han-Shi Hu, Guo-Jin Cao, Jun Li, and Lai-Sheng Wang

Citation: The Journal of Chemical Physics **140**, 094306 (2014); doi: 10.1063/1.4867278
View online: http://dx.doi.org/10.1063/1.4867278
View Table of Contents: http://scitation.aip.org/content/aip/journal/jcp/140/9?ver=pdfcov
Published by the AIP Publishing

Strong electron correlation in UO_2^-: A photoelectron spectroscopy and relativistic quantum chemistry study

Wei-Li Li,[1,a)] Jing Su,[2,3,a)] Tian Jian,[1] Gary V. Lopez,[1] Han-Shi Hu,[2] Guo-Jin Cao,[2] Jun Li,[2,b)] and Lai-Sheng Wang[1,c)]
[1]*Department of Chemistry, Brown University, Providence, Rhode Island 02912, USA*
[2]*Department of Chemistry & Key Laboratory of Organic Optoelectronics and Molecular Engineering of Ministry of Education, Tsinghua University, Beijing 100084, China*
[3]*Division of Nuclear Materials Science and Engineering, Shanghai Institute of Applied Physics, Chinese Academy of Sciences, Shanghai 201800, China and Key Laboratory of Nuclear Radiation and Nuclear Energy Technology, Chinese Academy of Sciences, Shanghai 201800, China*

(Received 20 September 2013; accepted 14 February 2014; published online 6 March 2014)

The electronic structures of actinide systems are extremely complicated and pose considerable challenges both experimentally and theoretically because of significant electron correlation and relativistic effects. Here we report an investigation of the electronic structure and chemical bonding of uranium dioxides, UO_2^- and UO_2, using photoelectron spectroscopy and relativistic quantum chemistry. The electron affinity of UO_2 is measured to be 1.159(20) eV. Intense detachment bands are observed from the UO_2^- low-lying $(7s\sigma_g)^2(5f\phi_u)^1$ orbitals and the more deeply bound O2*p*-based molecular orbitals which are separated by a large energy gap from the U-based orbitals. Surprisingly, numerous weak photodetachment transitions are observed in the gap region due to extensive two-electron transitions, suggesting strong electron correlations among the $(7s\sigma_g)^2(5f\phi_u)^1$ electrons in UO_2^- and the $(7s\sigma_g)^1(5f\phi_u)^1$ electrons in UO_2. These observations are interpreted using multi-reference *ab initio* calculations with inclusion of spin-orbit coupling. The strong electron correlations and spin-orbit couplings generate orders-of-magnitude more detachment transitions from UO_2^- than expected on the basis of the Koopmans' theorem. The current experimental data on UO_2^- provide a long-sought opportunity to arbitrating various relativistic quantum chemistry methods aimed at handling systems with strong electron correlations. © *2014 AIP Publishing LLC*. [http://dx.doi.org/10.1063/1.4867278]

I. INTRODUCTION

Actinide chemistry has attracted extensive research attention in recent years because of its increasing importance in nuclear industry and environmental science.[1] The electronic structures of actinide compounds are extremely complicated due to strong electron correlation and relativistic effects. While electronic spectroscopy is critical for characterizing the electronic structure of molecules, interpretation and assignment of such spectra for actinides are challenging because of experimental difficulties and the lack of accurate theoretical data on the electronic excited states. Application of standard electronic structure methods developed for weakly correlated systems to actinides with an open 5*f*-shell is either inappropriate or inefficient. Therefore, high resolution electronic spectra are keenly needed, in order to develop and calibrate electronic structure models suitable for actinide systems, in which electron-electron correlations are strong.

The UO_2 molecule has been an important model system for actinide chemistry and has been extensively studied both experimentally and theoretically.[2–16] UO_2 is known to be a linear molecule with a $^3\Phi_{2u}$ ground state and a $(7s\sigma_g)^1(5f\phi_u)^1$ electron configuration.[4–14] The ground-state vibrational frequencies of UO_2 were measured in rare gas matrices.[2–4] An interesting matrix effect, that leads to the so-called ground-state reversal, was observed, where the ground state of UO_2 in the Ar matrix was shown to have changed to a ^3H_g state with a $(5f\phi_u)^1(5f\delta_u)^1$ configuration owing to strong $(Ar)_x$-UO_2 interactions,[10,16] although such a state switching was not observed in fluorescence spectroscopy of UO_2 in an Ar matrix.[9] The electronic spectroscopy of gaseous UO_2 has also been studied, confirming its $^3\Phi_{2u}$ ground state and its first excited state of $^3\Phi_{3u}$ with an excitation energy of only 360 cm^{-1}.[8] A number of excited states of UO_2 have also been observed and compared with theoretical results.[5–9,12–14]

The linear UO_2 molecule is relevant to the uranium oxide solids used as nuclear fuels and it can also be viewed as the two-electron reduced version of the ubiquitous uranyl dication (UO_2^{2+}).[17] Despite the large number of studies on the UO_2 molecule and its excited states, relatively little is known about UO_2^-, in which the U atom is in an oxidation state of III. The UO_2^- anion was observed in a Ne matrix[4] and in the gas phase by mass spectrometry.[18,19] Its ground state was calculated to be $^2\Phi_u$ with a $(7s\sigma_g)^2(5f\phi_u)^1$ electron configuration.[4]

In this contribution, we report the first study of the UO_2^- anion using photoelectron spectroscopy (PES). PES is a powerful experimental technique to probe the electronic structure

[a)]W. L. Li and J. Su contributed equally to this work.
[b)]Electronic mail: junli@tsinghua.edu.cn.
[c)]Electronic mail: lai-sheng_wang@brown.edu.

of molecules, providing direct information about electronic states or approximately the one-electron energy levels as predicted by the molecular orbital (MO) theory. As a cornerstone of modern chemical bonding models, the MO theory is a triumph for quantum mechanics. The validity of the MO theory was confirmed by PES since the 1960s. The Koopmans' theorem, which states that the ionization energy is directly related to the MO energies ($IE_i = -\varepsilon_i$), is the bridge between PES and the MO theory. Despite its approximate nature, the Koopmans' theorem works surprisingly well for organic compounds, but breaks down frequently in inorganic compounds. In heavy-element systems, the failure of this theorem is expected, but it is difficult to be probed experimentally.

Here we show that the Koopmans' theorem breaks down severely for the electron detachment from UO_2^-, as a result of significant electron correlations. We report the first well-resolved PES spectra of UO_2^-, providing a wealth of experimental information on the excited states of the neutral UO_2 molecule, many of which are due to multi-electron transitions. We have performed highly accurate *ab initio* wave function theory (WFT) calculations using multi-configurational and the coupled cluster [CCSD(T)] approaches with corrections of scalar and spin-orbit coupling (SOC) relativistic effects to interpret the anion PE spectra. We show that the correlations are extremely strong between the U7*s* electrons in UO_2^-. Both the initial states (IS) and final states (FS) of the electron detachment from $UO_2^- \rightarrow e^- + UO_2$ have to be accurately calculated to understand the complicated PE spectra. The highly resolved PE spectra of UO_2^- thus provide a prototype for calibrating and benchmarking various relativistic quantum chemistry methods, especially those developed for systems with strong electron correlations.

II. EXPERIMENTAL AND THEORETICAL METHODS

A. Photoelectron spectroscopy

The experiment was carried out using a magnetic-bottle PES apparatus equipped with a laser vaporization cluster source, details of which have been published in Ref. 20. Briefly, a uranium disk (Goodfellow Corporation) was used as the laser-vaporization target. The residual oxygen contamination on the target surface was sufficient to produce the desired oxide clusters with a helium carrier gas, which was seeded with 5% Ar to achieve better supersonic cooling.[21,22] Negatively charged species were extracted from the cluster beam and analyzed in a time-of-fight mass spectrometer. The UO_2^- anions were mass-selected and decelerated before being photodetached by a laser beam at 193 nm (6.424 eV) from an ArF excimer laser, and 266 nm (4.661 eV), 355 nm (3.496 eV), or 532 nm (2.331 eV) from a Nd:YAG laser. Photoelectrons were collected at nearly 100% efficiency and analyzed in a 3.5 m long magnetic bottle. The resolution of the apparatus, $\Delta E_k/E_k$, was better than 2.5%, i.e., ~25 meV for 1 eV electrons.

B. Theoretical methods

Theoretical studies were carried out using both DFT and WFT methods. DFT calculations were performed on

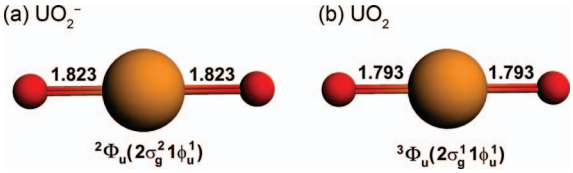

FIG. 1. Optimized structures of UO_2^- and UO_2 along with their point group symmetries, spectroscopic states, and electronic configurations. Bond lengths are given in Å.

UO_2^- and UO_2 using the generalized gradient approximation (GGA) with the PBE exchange-correlation functional[23] as implemented in the Amsterdam Density Functional (ADF 2010.02) program.[24–26] The Slater basis sets with the quality of triple-ζ plus two polarization functions (TZ2P)[27] were used, with the frozen core approximation applied to the inner shells [$1s^2$-$5d^{10}$] for U and [$1s^2$] for O. The scalar relativistic (SR) effects were taken into account by the zero-order-regular approximation (ZORA).[28] Geometries were fully optimized at the SR-ZORA level.

We further carried out WFT calculations using advanced *ab initio* electron correlation methods implemented in the MOLPRO 2012.1 program.[29] The coupled-cluster approach with single and double and perturbative triple excitations (CCSD(T))[30] and complete-active-space second order perturbation theory (CASPT2)[31] were used. The structures of UO_2^- and UO_2 were optimized at the level of CCSD(T) with the SR effects included (Fig. 1). Single-point CCSD(T) energies of the ground state of UO_2 were calculated at the optimized geometry of UO_2^-, which accurately generated the first VDE, indicating that the theoretical methods used are adequate. To obtain the higher VDEs, we used the CASPT2 method to calculate the ground and excited states of UO_2 at the CCSD(T) ground-state geometry of the anion. The active spaces for the ground- and excited-state CASSCF calculations of UO_2 include 13 orbitals from the U 5*f*, 6*d*, 7*s*, and 7*p* shells, i.e., $2\sigma_g$, $1\phi_u$, $1\delta_u$, $1\delta_g$, $2\pi_u$, $3\pi_u$, $2\sigma_u$, and $3\sigma_u$ (Figs. 2 and 3) with 2 valence electrons designated as CAS(2,13). This relatively small active space is only suitable for electron detachments involving intra-atomic electronic states, which are the focus of this work. SO-averaged CASPT2 calculations were performed on all the triplet and singlet states produced by this active space. Individually optimized state-averaged (SA) CASSCF orbitals were used for *gerade*(g)- and *ungerade*(u)-symmetry triplet and singlet states, respectively. In the CASPT2 calculations, the ionization potential electron affinity (IPEA)-corrected zeroth-order Hamiltonian[32] was used with an IPEA shift of 0.25 au. To avoid intruder states and improve CASPT2 convergence, a level shift of 0.2 au was applied. The U 6*s*6*p* and O 2*s*2*p* shells were correlated in the CASPT2 calculations. The SO coupling was treated by a state-interacting method[33,34] with SO pseudopotentials on the basis of SA-CASSCF wave functions of *g* and *u* symmetries, respectively. This is justified because *g* and *u* states do not mix under the influence of SO coupling. In the MOLPRO calculations, we used the Stuttgart energy-consistent relativistic 32-valence-electron pseudopotentials, ECP60MWB (U), and the corresponding ECP60MWB-SEG

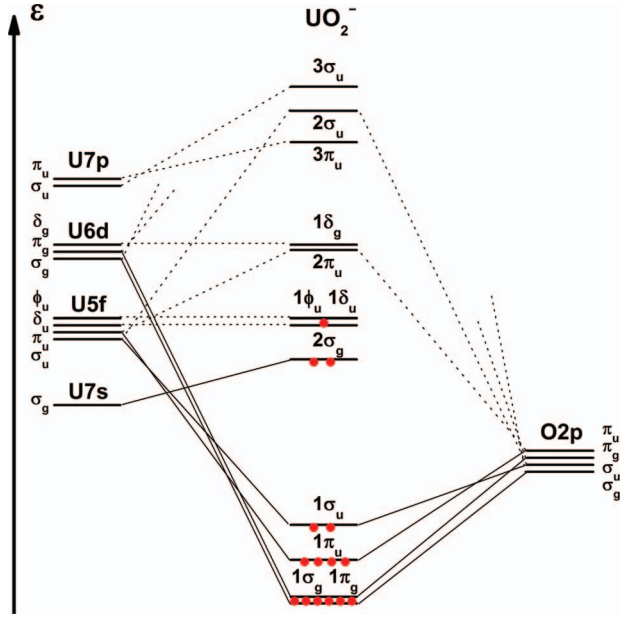

FIG. 2. Qualitative scalar-relativistic valence molecular orbital energy-level scheme for UO_2^-.

basis set for U[35–37] and the augmented polarized valence triple-ζ basis sets aug-cc-pVTZ for O.[38]

To evaluate the error of the truncated atomic basis sets on ground-state geometrical structures of UO_2^- and UO_2, we also performed CCSD(T) geometry optimization by employing a more accurate pseudopotential ECP60MDF and the corresponding basis sets of polarized valence quadruple-ζ quality for U[39] and the augmented polarized valence quadruple-ζ basis sets aug-cc-pVQZ for O.[38] The U–O bond length of UO_2^- and UO_2 increases by only 0.0076 Å and 0.0066 Å, respectively, showing that the atomic basis sets used are nearly converged toward the basis sets limit. The influence on geometrical structures from further basis set improvement can be neglected in this work.

III. RESULTS AND DISCUSSION

A. Photoelectron spectra of UO_2^-

The PE spectra of UO_2^- at four photon energies from 532 to 193 nm are shown in Fig. 4. At 193 nm (Fig. 4(d)),

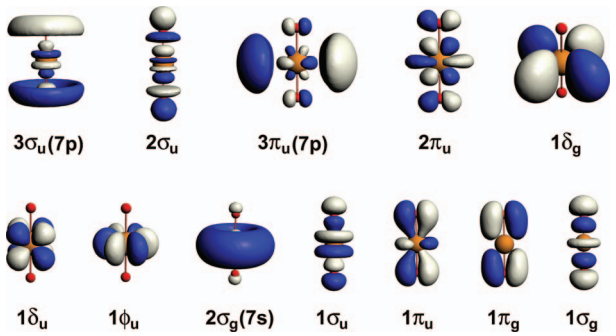

FIG. 3. Contour plots of the valence molecular orbitals (MOs) of UO_2^- at the DFT/PBE level (iso = 0.038 a.u.) with a $(2\sigma_u)^2(1\phi_u)^1$ electron configuration. The $1\phi_u$ orbital is the singly occupied MO and the $2\sigma_g$ orbital is the highest doubly occupied MO.

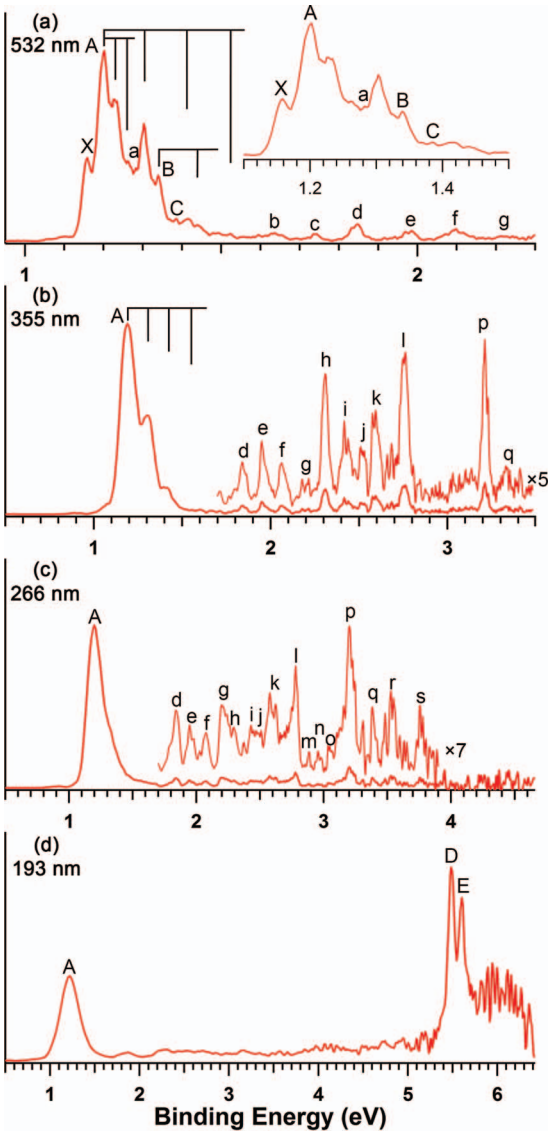

FIG. 4. Photoelectron spectra of UO_2^- at (a) 532 nm, (b) 355 nm, (c) 266 nm, and (d) 193 nm.

three strong PES bands are observed. The broad low binding energy band labeled as A should be due to electron detachments from the U-based non-bonding 7*s*5*f* orbitals, whereas the much higher binding energy bands D and E and the broad signals around 6 eV should be due to electron detachment from the deeper O2*p*-based bonding orbitals. Weak electron signals are also observed in the energy gap region between 1.5 and 5 eV in the 193 nm spectrum, but not well resolved. At 266 nm (Fig. 4(c)) and 355 nm (Fig. 4(b)), however, numerous sharp peaks are resolved for the weak signals above 1.5 eV in the energy gap region. The band A is also resolved in the 355 nm spectrum into a short vibrational progression (~890 cm^{-1}), which should be due to the symmetric stretching of UO_2.

At 532 nm (Fig. 4(a)), band A is further resolved into numerous fine features, which should be due to the overlap of several electronic states. The peak X resolved at the lowest binding energy of 1.159 eV should correspond to the ground-state transition, which defines the adiabatic detachment

TABLE I. Observed vertical detachment energies (VDEs) from the photoelectron spectra of UO_2^- and comparison with theoretical calculations at different levels of theory with inclusion of spin-orbit coupling.

		Current experiment		SO-CASPT2		ΔE from literature (cm^{-1})			
	Final state	VDEs (eV)[a]	ΔE (cm^{-1})[b]	VDE (eV)	ΔE (cm^{-1})[b]	Expt.[8,9]	IHFSCC[14]	GASCI[13]	CASPT2[12]
X	2_u	1.159 (20)	0	1.159[c]	0	0	0	0	0
A	3_u	1.202 (20)	350	1.204	362	360	368	427	378
a	4_g	1.282 (30)	990	1.283	1001		10 914[d]		3300
B	1_u	1.339 (20)	1450	1.367	1679	1094[e]	2231	1089	2567
C	2_u	1.384 (30)	1810	1.417	2083	1401[e]	2588	1542	2908
D	$^3\Phi_g$	5.485 (30)	34 890	5.587[f]	35 730				
E		5.604 (30)	35 850						

[a]Numbers in parentheses represent the uncertainty in the last two digits.
[b]Excitation energies of the excited states of UO_2 relative to the ground state.
[c]Theoretical results from the current work. The calculated first VDE is 1.097 eV. All higher VDEs are offset by 0.062 eV to facilitate comparison with the experimental data.
[d]This value is 3330 cm^{-1} (see last column) according to CASPT2 calculations in Ref. 12. It is primarily due to the completely different approach to electron correlation chosen in both methods.[14]
[e]The experimental excitation energies in an Ar matrix.[9]
[f]From CCSD(T) calculations.

energy (ADE) of UO_2^- or the electron affinity (EA) of neutral UO_2. The separation of peak X and the onset of band A at 1.202 eV, which should correspond to the first excited state of UO_2, is only 0.043 eV (350 cm^{-1}). This quantity is in excellent agreement with the excitation energy of the first excited state of gaseous UO_2 reported previously,[8] as compared in Table I. In addition to the stretching progression, which is measured more accurately at 532 nm as 870 ± 50 cm^{-1}, a lower frequency progression of 250 ± 30 cm^{-1} was also resolved for band A. As will be shown below, this progression is due to excitation of the even vibrational quanta of the bending mode in band A. Another well-resolved feature B at 1.339 eV is observed, which is assigned as a new detachment channel and contains a possible vibrational progression of 810 ± 50 cm^{-1}. One weaker feature C is observed with a VDE value of 1.384 eV and is assigned as another detachment channel. Feature *a* at 1.282 eV is observed and assigned as a new detachment transition. The features *a*, B, and C are assigned tentatively as distinct detachment channels because they cannot be assigned as any vibrational excitations for band A. These assignments are compared with the calculated results in Table I.

The most significant and surprising observation is the nearly continuous weak photodetachment signals observed between 1.5 and 5 eV in the 193 nm spectrum, which give rise to a set of congested but well-resolved peaks in the lower photon energy spectra (Figs. 4(a)–4(c)). Eighteen such peaks are tentatively identified up to 3.9 eV and labeled as *b*, *c*, … to *s*. No features are identified in the 4–5 eV range because of the low signal-to-noise ratios. The shapes and relative intensities of some of these weak features seem to vary with the detachment photon energies, suggesting that either there are more than one transitions in these features or they are wavelength-dependent. Because UO_2^- contains only three quasi-atomic U-based valence electrons ($7s^2 5f^1$), such a high density of detachment channels is not expected on the basis of the Koopmans' theorem. As shown below, these weak peaks are due to extensive two-electron detachment transitions, which are direct manifestation of the strong electron correlation effects in UO_2^- and the breakdown of the Koopmans' theorem. The VDEs of all the observed detachment transitions are summarized and compared with the theoretical data in Tables I and II.

B. Theoretical results and comparison with experiment

The optimized structures of UO_2^- and UO_2 at the level of CCSD(T) with the SR effects included are shown in Fig. 1. The U–O bond length in the anion is 1.823 Å, which is comparable to the previously reported value of 1.828 Å at DFT/B3LYP level.[4] Neutral UO_2 has an optimized U–O bond length of 1.793 Å at the SR level, which is close to the reported 1.806 Å at the SR-CASPT2 level.[5] Previous calculations show that inclusion of spin-orbit coupling does not change the U–O distance significantly. The U–O bond length is 1.80 Å at the SO-CI level,[6] 1.770 Å at the DC-FSCC level[14] and 1.766 Å at the SO-CASPT2 level.[5] While in general bond length depends on the atomic basis sets, electron correlation level, and spin-orbit coupling effect,[5,14] our calculations using a more accurate pseudopotential and larger basis set for U and O indicate that the U–O bond lengths in UO_2^- and UO_2 do not change substantially, showing the influence on geometrical structures from further basis set improvement can be neglected at this level of theory.

To understand and to interpret the PE spectra of UO_2^-, we performed extensive calculations of the ground and excited states of UO_2^- and neutral UO_2 at the optimized geometry of UO_2^-. Fig. 2 shows the qualitative SR energy levels of the Kohn-Sham valence orbitals of UO_2^-, and the corresponding MO contours are shown in Fig. 3. The U5*f* orbitals transform as $f\sigma_u(m = 0) + f\pi_u$ ($m = \pm 1$) + $f\delta_u$ ($m = \pm 2$) + $f\phi_u$ ($m = \pm 3$) in the $D_{\infty h}$ symmetry, where $5f\phi_u$ forms the $1\phi_u$ nonbonding MO and $5f\delta_u$ forms the $1\delta_u$ nonbonding MO in UO_2^-. The $1\phi_u$ and $1\delta_u$ MOs are almost degenerate in UO_2^- and UO_2 due to lack of orbital interaction with the ligands. The doubly occupied $2\sigma_g$ MO mainly consists of the U7*s* orbital. The unoccupied $5f\pi_u$ ($2\pi_u$) and $6d\delta_g$ ($1\delta_g$) MOs are only slightly higher in energy, whereas even higher lie the U7*p*-based orbitals ($3\pi_u$ and $3\sigma_u$) of

TABLE II. All the observed weak features from the photoelectron spectra and their comparison with the CASSCF/CASPT2/SO calculation results of UO_2^-.[a]

Feature	VDE (eV)	Calc. (eV)	E (cm^{-1})	ΔE (cm^{-1})	Ω	Compositions of SR states
X	1.159(20)	1.159	9356	0	2_u	89% $^3\Phi_u(2\sigma_g1\phi_u)$ + 8% $^3\Delta_u(2\sigma_g1\delta_u)$
A	1.202(20)	1.204	9718	362	3_u	51% $^3\Phi_u(2\sigma_g1\phi_u)$ + 36% $^1\Phi_u(2\sigma_g1\phi_u)$ + 13% $^3\Delta_u(2\sigma_g1\delta_u)$
a	1.282 (30)	1.283	10 357	1001	4_g	93% $^3H_g(\mathbf{1\phi_u1\delta_u})$
B	1.339(20)	1.367	11 035	1679	1_u	98% $^3\Delta_u(2\sigma_g1\delta_u)$
C	1.384(30)	1.417	11 439	2083	2_u	56% $^3\Delta_u(2\sigma_g1\delta_u)$ + 41% $^1\Delta_u(2\sigma_g1\delta_u)$
b	1.63(3)	1.571	12 679	3323	0_g	57% $^3\Sigma_g^-(1\delta_u{}^2 + \mathbf{1\phi_u{}^2})$ + 28% $^3\Pi_g(\mathbf{1\phi_u1\delta_u})$ + 15% $^1\Sigma_g^+(1\delta_u{}^2 + \mathbf{1\phi_u{}^2})$
c	1.74(4)	1.741	14 047	4691	1_g	48% $^3\Pi_g(\mathbf{1\phi_u1\delta_u})$ + 35% $^3\Sigma_g^-(1\delta_u{}^2 + \mathbf{1\phi_u{}^2})$ + 13% $^1\Pi_g(\mathbf{1\phi_u1\delta_u})$
		1.797	14 504	5148	5_g	99% $^3H_g(\mathbf{1\phi_u1\delta_u})$
		1.799	14 515	5159	4_u	100% $^3\Phi_u(2\sigma_g1\phi_u)$
d	1.85(3)	1.840	14 850	5494	3_u	47% $^3\Phi_u(2\sigma_g1\phi_u)$ + 29% $^3\Delta_u(2\sigma_g1\delta_u)$ + 24% $^1\Phi_u(2\sigma_g1\phi_u)$
		1.878	15 158	5802	3_u	57% $^3\Delta_u(2\sigma_g1\delta_u)$ + 40% $^1\Phi_u(2\sigma_g1\phi_u)$ + 2% $^3\Phi_u(2\sigma_g1\phi_u)$
		1.881	15 176	5820	4_u	92% $^3H_u(\mathbf{1\phi_u1\delta_g})$
e	1.98(4)	1.916	15 463	6107	2_u	55% $^1\Delta_u(2\sigma_g1\delta_u)$ + 35% $^3\Delta_u(2\sigma_g1\delta_u)$ + 10% $^3\Phi_u(2\sigma_g1\phi_u)$
		2.013	16 247	6891	0_u	67% $^1\Sigma_u^-(1\delta_u1\delta_g)$ + 31% $^3\Sigma_u^+(1\delta_u1\delta_g)$
f	2.10(3)	2.116	17 074	7718	3_u	98% $^3\Gamma_u(1\delta_u1\delta_g)$
		2.167	17 487	8131	1_g	61% $^3\Sigma_g^-(\mathbf{1\phi_u{}^2} + 1\delta_u{}^2)$ + 21% $^1\Pi_g(\mathbf{1\phi_u1\delta_u})$ + 15% $^3\Pi_g(\mathbf{1\phi_u1\delta_u})$
g	2.22(4)	2.175	17 552	8196	0_g	100% $^3\Pi_g(\mathbf{1\phi_u1\delta_u})$
		2.214	17 864	8508	6_g	95% $^3H_g(\mathbf{1\phi_u1\delta_u})$
		2.257	18 214	8858	5_u	85% $^3H_u(\mathbf{1\phi_u1\delta_g})$ + 12% $^3\Gamma_u(1\delta_u1\delta_g)$
h	2.31(3)	2.263	18 259	8903	2_g	93% $^3\Pi_g(\mathbf{1\phi_u1\delta_u})$
		2.277	18 371	9015	1_u	40% $^3\Pi_u(\mathbf{1\phi_u1\delta_g})$ + 28% $^3\Sigma_u^+(1\delta_u1\delta_g)$ + 28% $^1\Pi_u(\mathbf{1\phi_u1\delta_g})$
		2.305	18 603	9247	0_g	63% $^3\Pi_g(\mathbf{1\phi_u1\delta_u})$ + 25% $^1\Sigma_g^+(1\delta_u{}^2 + \mathbf{1\phi_u{}^2})$
		2.408	19 428	10 072	0_u	65% $^3\Pi_u(\mathbf{1\phi_u1\delta_g})$ + 24% $^3\Sigma_u^+(1\delta_u1\delta_g)$ + 11% $^1\Sigma_u^-(1\delta_u1\delta_g)$
i	2.42(4)	2.416	19 491	10 135	4_g	87% $^1\Gamma_g(1\delta_u{}^2)$
		2.455	19 809	10 453	4_u	88% $^3\Gamma_u(1\delta_u1\delta_g)$ + 5%a$^1\Gamma_u(1\delta_u1\delta_g)$ + 5%a$^3H_u(\mathbf{1\phi_u1\delta_g})$
		2.473	19 955	10 599	3_g	93% $^3\Gamma_g(\mathbf{1\phi_u3\pi_u})$
j	2.52(4)	2.505	20 209	10 853	1_u	58% $^3\Sigma_u^+(1\delta_u1\delta_g)$ + 24% $^3\Sigma_u^-(1\delta_u1\delta_g)$ + 10% $^1\Pi_u(\mathbf{1\phi_u1\delta_g})$
		2.509	20 247	10 891	0_u	86% $^3\Pi_u(\mathbf{1\phi_u1\delta_g})$ + 13% $^3\Sigma_u^-(1\delta_u1\delta_g)$
k	2.58(4)	2.609	21 052	11 696	0_g	59% $^3\Sigma_g^-(\mathbf{1\phi_u{}^2})$ + 18% $^1\Sigma_g^+(1\delta_u{}^2 + \mathbf{1\phi_u{}^2} + 1\delta_g{}^2 + 2\sigma_g{}^2)$ + 12% $^1\Sigma_g^+(1\delta_u{}^2 + \mathbf{1\phi_u{}^2})$+ 12% $^1\Sigma_g^+(1\delta_u{}^2 + \mathbf{1\phi_u{}^2})$
		2.615	21 097	11 741	0_u	66% $^3\Sigma_u^-(1\delta_u1\delta_g)$ + 22% $^1\Sigma_u^+(1\delta_u1\delta_g)$ + 9% $^3\Pi_u(\mathbf{1\phi_u1\delta_g})$
		2.747	22 166	12 810	6_u	100% $^3H_u(\mathbf{1\phi_u1\delta_g})$
		2.773	22 377	13 021	2_g	51% $^3\Phi_g(1\delta_u3\pi_u)$ + 21% $^1\Delta_g(\mathbf{1\phi_u3\pi_u})$ + 21% $^3\Delta_g(\mathbf{1\phi_u3\pi_u})$
l	2.76(3)	2.807	22 651	13 295	5_u	85% $^3\Gamma_u(1\delta_u1\delta_g)$ + 14% $^3H_u(\mathbf{1\phi_u1\delta_g})$
		2.822	22 772	13 416	1_g	43% $^3\Sigma_g^-(\mathbf{1\phi_u{}^2})$ + 30% $^1\Pi_g(\mathbf{1\phi_u1\delta_u})$ + 22% $^3\Pi_g(\mathbf{1\phi_u1\delta_u})$
		2.826	22 799	13 443	2_g	45% $^3\Phi_g(1\delta_u3\pi_u)$ + 25% $^3\Delta_g(\mathbf{1\phi_u3\pi_u})$ + 22% $^1\Delta_g(\mathbf{1\phi_u3\pi_u})$
		2.829	22 826	13 470	0_g	46% $^1\Sigma_g^+(1\delta_u{}^2 + \mathbf{1\phi_u{}^2})$ + 27% $^3\Sigma_g^-(1\delta_u{}^2 + \mathbf{1\phi_u{}^2})$ + 11% $^3\Sigma_g^-(\mathbf{1\phi_u{}^2})$
		2.867	23 128	13 772	0_u	43% $^3\Sigma_u^+(1\delta_u1\delta_g)$ + 35% $^3\Pi_u(1\phi_u1\delta_g)$ + 20% $^1\Sigma_u^-(1\delta_u1\delta_g)$
m	2.88(5)	2.869	23 149	13 793	1_u	68% $^3\Sigma_u^-(1\delta_u1\delta_g)$ + 15% $^3\Pi_u(1\phi_u1\delta_g)$ + 13% $^3\Sigma_u^+(1\delta_u1\delta_g)$
		2.881	23 248	13 892	2_u	100% $^3\Pi_u(\mathbf{1\phi_u1\delta_g})$
n	2.95(5)	2.964	23 917	14 561	4_g	93% $^3\Gamma_g(\mathbf{1\phi_u3\pi_u})$
o	3.04(5)	3.014	24 319	14 963	4_u	92% $^1\Gamma_u(1\delta_u1\delta_g)$ + 4% $^3\Gamma_u(1\delta_u1\delta_g)$
		3.035	24 486	15 130	1_g	50% $^3\Sigma_g^-(\mathbf{1\phi_u{}^2})$ + 32% $^1\Pi_g(\mathbf{1\phi_u1\delta_u})$
		3.142	25 348	15 992	1_g	83% $^3\Delta_g(\mathbf{1\phi_u3\pi_u})$ + 9% $^3\Pi_g(\mathbf{1\phi_u1\delta_u})$
		3.168	25 558	16 202	1_u	53% $^1\Pi_u(\mathbf{1\phi_u1\delta_g})$ + 35% $^3\Pi_u(\mathbf{1\phi_u1\delta_g})$
		3.187	25 713	16 357	6_g	95% $^1I_g(\mathbf{1\phi_u{}^2})$
p	3.21(3)	3.213	25 919	16 563	3_g	92% $^3\Phi_g(1\delta_u3\pi_u)$
		3.214	25 930	16 574	0_u	96% $^3\Pi_u(2\sigma_g2\pi_u + 2\sigma_g3\pi_u)$
		3.224	26 013	16 657	0_u	97% $^3\Pi_u(2\sigma_g2\pi_u + 2\sigma_g3\pi_u)$
		3.283	26 485	17 129	3_g	94% $^3\Delta_g(\mathbf{1\phi_u3\pi_u})$
		3.305	26 665	17 309	1_u	64% $^3\Pi_u(2\sigma_g2\pi_u + 2\sigma_g3\pi_u)$ + 25% $^1\Pi_u(2\sigma_g2\pi_u)$

TABLE II. (*Continued*.)

Feature	VDE (eV)	Calc. (eV)	E (cm^{-1})	ΔE (cm^{-1})	Ω	Compositions of SR states
q	3.31	3.327	26 846	17 490	5_g	75% $^3\Gamma_g(\mathbf{1\phi_u 3\pi_u})$ + 25% $^1H_g(\mathbf{1\phi_u 1\delta_u})$
		3.360	27 110	17 754	1_g	64% $^3\Pi_g(1\delta_u 3\pi_u)$ + 28% $^1\Pi_g$ $(1\delta_u 3\pi_u)$
		3.521	28 410	19 054	0_u	73% $^1\Sigma_u^+(1\delta_u 1\delta_g)$ + 19% $^3\Sigma_u^-(1\delta_u 1\delta_g)$
		3.560	28 723	19 367	2_u	98% $^3\Pi_u(2\sigma_g 2\pi_u + 2\sigma_g 3\pi_u)$
		3.565	28 759	19 403	5_u	96% $^1H_u(\mathbf{1\phi_u 1\delta_g})$
r	3.53(5)	3.624	29 239	19 883	0_g	100% $^3\Pi_g(1\delta_u 3\pi_u)$
		3.638	29 349	19 993	2_g	62% $^3\Pi_g(1\delta_u 3\pi_u)$ + 26% $^3\Delta_g$ $(1\phi_u 3\pi_u)$
		3.638	29 350	19 994	4_g	90% $^3\Phi_g(1\delta_u 3\pi_u)$
		3.644	29 396	20 040	1_u	66% $^1\Pi_u(2\sigma_g 2\pi_u)$ + 24% $^3\Pi_u(2\sigma_g 2\pi_u + 2\sigma_g 3\pi_u)$
		3.645	29 410	20 054	0_g	80% $^3\Pi_g(1\delta_u 3\pi_u)$ + 13% $^3\Sigma_g^-(1\phi_u{}^2)$
		3.699	29 843	20 487	0_g	72% $^1\Sigma_g^+(1\delta_u{}^2 + \mathbf{1\phi_u{}^2} + 1\delta_g{}^2 + 2\sigma_g{}^2)$ + 16% $^3\Sigma_g^-(\mathbf{1\phi_u{}^2})$
		3.751	30 265	20 909	5_g	75% $^1H_g(\mathbf{1\phi_u 1\delta_u})$ + 24% $^3\Gamma_g(\mathbf{1\phi_u 3\pi_u})$
		3.785	30 540	21 184	2_g	46% $^1\Delta_g(\mathbf{1\phi_u 3\pi_u})$ + 30% $^3\Pi_g(1\delta_u 3\pi_u)$ + 20% $^3\Delta_g(\mathbf{1\phi_u 3\pi_u})$
s	3.76(4)	3.797	30 632	21 276	1_g	95% $^3\Delta_g(\mathbf{1\phi_u 2\pi_u} + 2\sigma_g 1\delta_g)$
		3.818	30 799	21 443	2_u	99% $^3\Phi_u(1\delta_g 2\pi_u + 1\delta_g 3\pi_u + \mathbf{1\phi_u 2\sigma_g})$
		3.844	31 012	21 656	4_g	93% $^1\Gamma_g(\mathbf{1\phi_u 3\pi_u} + 1\delta_u{}^2)$
		3.922	31 642	22 286	2_g	88% $^3\Delta_g(\mathbf{1\phi_u 2\pi_u} + 2\sigma_g 1\delta_g)$

[a]The leading configurations are shown in bold face.

Rydberg character and the $5f\sigma_u$ $(2\sigma_u)$ MO of anti-bonding character. Without SO coupling the UO_2^- anion has a $^2\Phi_u$ ground state with a $(2\sigma_g)^2(1\phi_u)^1$ electron configuration.[4] The first excited state $^2\Delta_u$ with a $(2\sigma_g)^2(1\delta_u)^1$ electron configuration lies 0.11 eV above the ground state. All the oxygen valence electrons participate in the two U≡O triple bonds, forming the four deeper and fully occupied MOs ($1\sigma_u$, $1\pi_u$, $1\sigma_g$, and $1\pi_g$), which are similar to those in uranyl (UO_2^{2+}).[1,17,40–44] These ligand-based MOs are well separated from the U(7*s*5*f*)-based MOs and are primarily composed of O(2*p*) atomic orbitals with some mixing of the U(5*f*6*d*) orbitals as a result of U–O orbital interactions.

According to group theory, the $^2\Phi_u$ $(2\sigma_g{}^2 1\phi_u{}^1)$ and $^2\Delta_u$ $(2\sigma_g{}^2 1\delta_u{}^1)$ states will mix under SO coupling, yielding four new SOC states: $^2\Phi_{5/2u}$, $^2\Delta_{3/2u}$, $^2\Phi_{7/2u}$, and $^2\Delta_{5/2u}$. Their wavefunctions and relative energies from our SO-CASPT2 calculations are shown in Table III. The wavefunction of the ground state $^2\Phi_{5/2u}$ is (88% $^2\Phi_u$ + 12% $^2\Delta_u$) with the SR ground state $^2\Phi_u$ dominant. The first excited state $^2\Delta_{3/2u}$ $(2\sigma_g{}^2 1\delta_u{}^1)$ is 0.26 eV higher at the SO-CASPT2 level (Table III). Such a high anionic excited state is unlikely to be populated at room temperature, thus ruling out its presence in the experiment. Inasmuch as the ground state $^2\Phi_{5/2u}$ [88% $^2\Phi_u$ $(2\sigma_g{}^2 1\phi_u{}^1)$ + 12% $^2\Delta_u$ $(2\sigma_g{}^2 1\delta_u{}^1)$] of UO_2^- mainly involves the $2\sigma_g{}^2 1\phi_u{}^1$ electron configuration, UO_2^- should produce three major detachment channels on the basis of Koopmans' theorem:

$$UO_2^- : 2\sigma_g{}^2 1\phi_u{}^1(^2\Phi_{5/2u}) \rightarrow UO_2 : 2\sigma_g{}^1 1\phi_u{}^1(^3\Phi_{2u,3u,4u}), \quad (1)$$

$$\rightarrow 2\sigma_g{}^1 1\phi_u{}^1(^1\Phi_{3u}), \quad (2)$$

$$\rightarrow 2\sigma_g{}^2 1\phi_u{}^0(^1\Sigma_{0g}^+). \quad (3)$$

Detachment from the deeper O2*p*-based MOs would produce energetically much higher excited states of UO_2. This picture qualitatively agrees with the 193 nm PE spectrum (Fig. 4(d)). In particular, the features D and E should be due to detachment from the $1\sigma_u$ MO, corresponding to the triplet $^3\Phi_g$ $(1\sigma_u{}^1 2\sigma_g{}^2 1\phi_u{}^1)$ and singlet $^1\Phi_g$ $(1\sigma_u{}^1 2\sigma_g{}^2 1\phi_u{}^1)$ final UO_2 states, respectively. Thus, the X-D separation of 4.326 eV (34 890 cm^{-1}) should correspond to the lowest ligand-to-metal electronic excitation energy in UO_2 $(X^3\Phi_u \rightarrow {}^3\Phi_g)$. Our calculated VDE for the triplet final state is 5.587 eV, in excellent agreement with the experimental value of 5.485 eV (Table I).

However, the one-electron MO picture at the Hartree-Fock or approximate Kohn-Sham levels and the Koopmans' theorem, involving only the initial state of the electron detachment, break down severely and cannot interpret the numerous fine PES features observed for UO_2^-, suggesting strong electron correlation effects. These multi-electron processes are called shakeup in PES.[45] Thus, the UO_2 final states with the inclusion of multi-reference configuration mixing and relativistic effects including SO coupling have to be considered, in order to understand the PE spectra.

TABLE III. The ground state and the lowest excited states of UO_2^-. Vertical excitation energies (ΔE in eV) at the CASSCF/X/SO (X = CCSD(T), CASPT2) level and the SR-CCSD(T)-optimized ground-state geometry (Fig. 1).

	CASSCF/CCSD(T)/SO		CASSCF/CASPT2/SO[a]	
SO state	Composition of SR states	ΔE	Composition of SR states	ΔE
5/2u	89%$^2\Phi_u$ + 11%$^2\Delta_u$	0	88%$^2\Phi_u$ + 12%$^2\Delta_u$	0
3/2u	100%$^2\Delta_u$	0.29	100%$^2\Delta_u$	0.26
7/2u	100%$^2\Phi_u$	0.67	100%$^2\Phi_u$	0.67
5/2u	89%$^2\Delta_u$ + 11%$^2\Phi_u$	0.76	88%$^2\Delta_u$ + 12%$^2\Phi_u$	0.74

[a]With an active space of CAS(2,13).

TABLE IV. The calculated vertical excitation energies of UO_2 at the SR CASPT2 level.[a]

State	Main configurations (leading in bold)	ΔE (eV)	ΔE (cm^{-1})
$a^3\Phi_u$	$2\sigma_g 1\phi_u$ ($7s5f_\phi$)	0.0000	0
$a^3\Delta_u$	$2\sigma_g 1\delta_u$ ($7s5f_\delta$)	0.0735	593
$a^1\Phi_u$	$2\sigma_g 1\phi_u$ ($7s5f_\phi$)	0.1135	916
$a^1\Delta_u$	$2\sigma_g 1\delta_u$ ($7s5f_\delta$)	0.1888	1523
a^3H_g	$1\delta_u 1\phi_u$ ($5f_\delta 5f_\phi$)	0.3037	2449
$a^3\Sigma_g^-$	$1\delta_u{}^2 + 1\phi_u{}^2$ ($5f_\delta 5f_\delta + 5f_\phi 5f_\phi$)	0.5363	4325
$a^3\Pi_g$	$\mathbf{1\delta_u 1\phi_u} + 1\delta_u 2\pi_u + 1\delta_u 3\pi_u$ ($\mathbf{5f_\delta 5f_\phi} + 5f_\delta 5f_\pi + 5f_\delta 7p_\pi$)	0.7380	5953
$a^1\Sigma_u^-$	$1\delta_u 1\delta_g$ ($5f_\delta 6d_\delta$)	0.7399	5968
a^3H_u	$1\phi_u 1\delta_g$ ($5f_\phi 6d_\delta$)	0.8280	6678
$a^1\Gamma_g$	$\mathbf{1\delta_u{}^2} + 1\phi_u 3\pi_u + 1\phi_u 2\pi_u$ ($\mathbf{5f_\delta{}^2} + 5f_\phi 7p_\pi + 5f_\phi 5f_\pi$)	0.9176	7401
$a^3\Gamma_u$	$1\delta_u 1\delta_g$ ($5f_\delta 6d_\delta$)	0.9411	7591
$a^3\Sigma_u^+$	$1\delta_u 1\delta_g$ ($5f_\delta 6d_\delta$)	0.9882	7970
$a^1\Sigma_g^+$	$1\delta_u{}^2 + 1\phi_u{}^2$ ($5f_\delta{}^2 + 5f_\phi{}^2$)	0.9904	7988
$a^1\Pi_g$	$\mathbf{1\delta_u 1\phi_u} + 1\delta_u 2\pi_u + 1\delta_u 3\pi_u$ ($\mathbf{5f_\delta 5f_\phi} + 5f_\delta 5f_\pi + 5f_\delta 7p_\pi$)	1.1101	8954
$a^3\Pi_u$	$\mathbf{1\phi_u 1\delta_g} + 2\sigma_g 2\pi_u + 2\sigma_g 3\pi_u$ ($\mathbf{5f_\phi 6d_\delta} + 7s5f_\pi + 7s7p_\pi$)	1.2090	9751
$a^3\Sigma_u^-$	$1\delta_u 1\delta_g$ ($5f_\delta 6d_\delta$)	1.2772	10 301
$a^1\Pi_u$	$\mathbf{1\phi_u 1\delta_g} + 2\sigma_g 2\pi_u + 1\delta_g 2\pi_u$ ($\mathbf{5f_\phi 6d_\delta} + 7s5f_\pi + 6d_\delta 5f_\pi$)	1.3429	10 831
$b^3\Sigma_g^-$	$\mathbf{1\phi_u{}^2} + 1\delta_g{}^2 + 1\delta_u{}^2$ ($\mathbf{5f_\phi 5f_\phi} + 6d_\delta 6d_\delta + 5f_\delta 5f_\delta$)	1.4427	11 636
$a^1\Gamma_u$	$1\delta_u 1\delta_g$ ($5f_\delta 6d_\delta$)	1.4764	11 908
$a^3\Gamma_g$	$\mathbf{1\phi_u 3\pi_u} + 1\phi_u 2\pi_u$ ($\mathbf{5f_\phi 7p_\pi} + 5f_\phi 5f_\pi$)	1.4851	11 978
a^1I_g	$1\phi_u{}^2$ ($5f_\phi{}^2$)	1.6178	13 049
$a^3\Phi_g$	$\mathbf{1\delta_u 3\pi_u} + 1\delta_u 2\pi_u$ ($\mathbf{5f_\delta 7p_\pi} + 5f_\delta 5f_\pi$)	1.7112	13 802
$a^3\Delta_g$	$\mathbf{1\phi_u 3\pi_u} + 1\phi_u 2\pi_u + 2\sigma_g 1\delta_g$ ($\mathbf{5f_\phi 7p_\pi} + 5f_\phi 5f_\pi + 7s6d_\delta$)	1.7188	13 863
$a^1\Sigma_u^+$	$1\delta_u 1\delta_g$ ($5f_\delta 6d_\delta$)	1.8121	14 616
$a^1\Delta_g$	$\mathbf{1\phi_u 3\pi_u} + 1\phi_u 2\pi_u + 2\sigma_g 1\delta_g$ ($\mathbf{5f_\phi 7p_\pi} + 5f_\phi 5f_\pi + 7s6d_\delta$)	1.8582	14 987
$b^3\Pi_u$	$2\sigma_g 2\pi_u + 2\sigma_g 3\pi_u$ ($7s5f_\pi + 7s7p_\pi$)	1.8764	15 134
$b^1\Sigma_g^+$	$1\delta_u{}^2 + 1\phi_u{}^2 + 1\delta_g{}^2 + 2\sigma_g{}^2$ ($5f_\delta{}^2 + 5f_\phi{}^2 + 6d_\delta{}^2 + 7s^2$)	1.9140	15 437
a^1H_u	$1\phi_u 1\delta_g$ ($5f_\phi 6d_\delta$)	2.0002	16 133
$b^1\Pi_u$	$\mathbf{2\sigma_g 2\pi_u} + 2\sigma_g 3\pi_u + 1\delta_g 2\pi_u + 1\delta_g 3\pi_u$ ($\mathbf{7s5f_\pi} + 7s7p_\pi + 6d_\delta 5f_\pi + 6d_\delta 7p_\pi$)	2.0673	16 674
a^1H_g	$1\delta_u 1\phi_u$ ($5f_\delta 5f_\phi$)	2.1340	17 212
$b^3\Pi_g$	$\mathbf{1\delta_u 3\pi_u} + 1\delta_u 1\phi_u + 1\delta_u 2\pi_u$ ($\mathbf{5f_\delta 7p_\pi} + 5f_\delta 5f_\phi + 5f_\delta 5f_\pi$)	2.1590	17 413
$b^1\Gamma_g$	$1\phi_u 3\pi_u + 1\delta_u{}^2$ ($5f_\phi 7p_\pi + 5f_\delta{}^2$)	2.3748	19 154
$b^1\Pi_g$	$\mathbf{1\delta_u 3\pi_u} + 1\delta_u 1\phi_u + 1\delta_u 2\pi_u$ ($\mathbf{5f_\delta 7p_\pi} + 5f_\delta 5f_\phi + 5f_\delta 5f_\pi$)	2.4876	20 064
$b^3\Delta_g$	$1\phi_u 2\pi_u + 2\sigma_g 1\delta_g$ ($5f_\phi 5f_\pi + 7s6d_\delta$)	2.5024	20 183
$b^3\Phi_u$	$1\delta_g 2\pi_u + 1\delta_g 3\pi_u + 2\sigma_g 1\phi_u$ ($6d_\delta 5f_\pi + 6d_\delta 7p_\pi + 7s5f_\phi$)	2.6068	21 026
$c^3\Pi_u$	$1\delta_g 2\pi_u + 1\delta_g 3\pi_u + 2\sigma_g 2\pi_u$ ($6d_\delta 5f_\pi + 6d_\delta 7p_\pi + 7s5f_\pi$)	2.6846	21 652
$a^1\Phi_g$	$1\delta_u 3\pi_u + 1\delta_u 2\pi_u$ ($5f_\delta 7p_\pi + 5f_\delta 5f_\pi$)	2.8265	22 798
$b^1\Phi_u$	$\mathbf{1\delta_g 2\pi_u} + 1\delta_g 3\pi_u + 2\sigma_g 1\phi_u$ ($\mathbf{6d_\delta 5f_\pi} + 6d_\delta 7p_\pi + 7s5f_\phi$)	2.8850	23 269
$c^1\Sigma_g^+$	$2\sigma_g{}^2 + 1\delta_g{}^2 + 1\phi_u{}^2$ ($\mathbf{7s^2} + 6d_\delta{}^2 + 5f_\phi{}^2$)	2.9083	23 457
$c^1\Pi_u$	$\mathbf{1\delta_g 2\pi_u} + 1\delta_g 3\pi_u + 2\sigma_g 2\pi_u + 1\delta_g 1\phi_u$ ($\mathbf{6d_\delta 5f_\pi} + 6d_\delta 7p_\pi + 7s5f_\pi + 6d_\delta 5f_\phi$)	2.9220	23 567

[a]The leading configurations are shown in bold face.

At the SR level, the CASPT2 calculations of UO_2 show that the $^3\Phi_u$ state is the ground state with a $2\sigma_g{}^1 1\phi_u{}^1$ electron configuration. Three low-lying states ($^3\Delta_u$, $^1\Phi_u$, and $^1\Delta_u$) derived from the $2\sigma_g{}^1(1\phi_u, 1\delta_u)^1$ electron configuration are shown in Table IV, along with their relative energies to the ground state. The ^3H_g state with a $(1\delta_u)^1(1\phi_u)^1$ ($5f\phi 5f\delta$) electron configuration, which was suggested to be the matrix-induced ground state in the Ar matrix study of UO_2,[10,16] lies 2449 cm^{-1} above the ground state. DFT calculations without SO coupling show that the ^3H_g state is 1920 cm^{-1} (Ref. 4) above the $^3\Phi_u$ ground state. At the SR-CASPT2 level, this energy difference is calculated to be 5954 cm^{-1} (Ref. 12). At the spin-free DC-IHFSCC level of theory, the ^3H_g state is found to be 12 863 cm^{-1} above the $^3\Phi_u$ ground state.[14]

Upon including SO coupling, the ground state $^3\Phi_u$ and excited states $^3\Delta_u$, $^1\Phi_u$, $^1\Delta_u$ split into states with Ω values of 4, 3, 2 ($^3\Phi_u$), 3, 2, 1 ($^3\Delta_u$), 3 ($^1\Phi_u$), and 2 ($^1\Delta_u$). Our calculations show that the 2_u state, whose wavefunction is ($89\%{}^3\Phi_u + 8\%{}^3\Delta_u$), is the SO-coupled ground state (Table II). The first VDE corresponding to $UO_2{}^-$ ($X^2\Phi_{5/2u}$) → UO_2 ($X^3\Phi_{2u}$)

is calculated to be 1.097 eV at the CASSCF/CCSD(T)/SO level of theory,[46] only 0.062 eV smaller than the experimental VDE (1.159 eV) measured for the ground-state detachment band X. To simplify the comparison between the experimental and calculated values, all the calculated VDEs are offset by 0.062 eV in Tables I and II. The calculated VDEs for the 3_u, 1_u, and 2_u states after the 0.062 eV offset are 1.204, 1.367, and 1.417 eV, in excellent agreement with the measured VDEs for bands A (1.202 eV), B (1.339 eV), and C (1.384 eV), respectively (Table I). The excitation energy of the 3_u state (350 cm^{-1}) obtained from the current PES work agrees well with the previous value (360 cm^{-1}) measured by the Heaven group for gaseous UO_2.[8] As compared in Table I, the excitation energies obtained for the 1_u and 2_u states in the current study seem to be slightly higher than those obtained by the Heaven group for UO_2 isolated in an Ar matrix,[9] probably due to the approximation in CASPT2 and/or the non-negligible matrix effects. The calculated excitation energies for the 3_u, 1_u, and 2_u states from several recent theoretical studies[12–14] are also given in Table I for comparison.

The weak feature *a* observed at 1.282 eV (Fig. 4(a) and Table I) is tentatively assigned to the lowest 4_g state with a calculated VDE of 1.283 eV. There is no other low-lying state below the 4_g state, in addition to the 3_u state. Hence, the two peaks between the origin of the A band and the feature *a* are assigned to the even quanta of the bending mode for the 3_u state of UO_2. The average measured spacing is 250 $\pm$ 30 cm^{-1}, which gives a bending frequency of ~125 cm^{-1}, in agreement with the 129 cm^{-1} bending frequency measured for the 3_u state by the Heaven group.[8] The ground-state detachment band X may also contain vibrational excitations. However, the relatively weaker intensity of the X band suggests that any vibrational peaks in the X band are likely to be buried under the features of the A band.

As mentioned above, the lowest 4_g state was suggested previously to be the ground state of UO_2 due to weak $(Ar)_x$-UO_2 bonding in an Ar matrix.[10,16] In our SO-CASPT2 calculation, the 4_g state relative to the 2_u ground state is 1001 cm^{-1} higher in energy. The SOCI calculations show that the 4_g state is 1642 cm^{-1} above the ground state.[6] However, the previous calculations listed in Table I tend to give larger excitation energy of this state. The SO-CASPT2 calculations give the excitation energy to be 3330 cm^{-1} (Ref. 12), which used a different active space from this work. The DC-IHFSCC method in Ref. 14 has given the 4_g state 10 914 cm^{-1} above the 2_u ground state, while the DC-CCSD(T) calculations give a result of 6991 cm^{-1}. One possible reason for the different calculated energies of the 4_g state is the use of different bond lengths. In our study, the single-point calculation of neutral UO_2 is performed using the anionic geometry (U–O distance: 1.823 Å) for vertical transitions, as measured in PES. However, calculations in the literature used the neutral optimized geometry with the U–O bond length varying from 1.770 Å to 1.827 Å.[6,12,14] Recalculating the vertical excitation of UO_2 at 1.770 Å gives the excitation energy of 4_g as 2942 cm^{-1}, which is in much better agreement with the SO-CASPT2 (Ref. 12) and DC-CCSD(T) results (Ref. 14), but is still different substantially from the DC-IHFSCC results of Ref. 14. The relatively smaller effect of bond length on the 4_g state has also been noted in Ref. 14, and the electron correlation is suggested to be more responsible for the discrepancy. As found in a previous SR-CASPT2 calculation,[12] in general different active spaces give different energy orderings and energy gaps among electronic states. Larger active spaces with accounting for more non-dynamic and dynamic electron correlations give more accurate results, but are often computationally impractical. Besides, the DC-CCSD(T) calculation of the excitation energy of the 4_g state gives an energy 1464 cm^{-1} higher than the DC-CCSD result in Ref. 14, showing the effect of dynamic electron correlations.

It is worth mentioning that in Ref. 14 the lowest 4_u state from the $5f\phi6d\delta$ configuration was found at 5047 cm^{-1} above the ground state, which is 5867 cm^{-1} lower than the 4_g state above. It was proposed to likely play an important role in the UO_2 chemistry in the Ar matrix. However, our SO-CASPT2 calculations show this 4_u state to be 4821 cm^{-1} higher than the 4_g state at the U–O bond length of 1.823 Å (3288 cm^{-1} at 1.770 Å), not supporting the proposition above.

Because of the complicated nature of the PE spectra of UO_2^-, the above assignment is only semi-quantitative due to the approximation of the SO-CASPT2 approach and the relatively small CAS(2,13) active space used. Clearly the calculated excited-state energies significantly depend on the level of electron correlation and relativistic effects, in addition to the quality of the atomic basis sets. Evaluation of more accurate excited state energies would require much larger active space involving even higher-energy U orbitals and ligand-based orbitals and higher-level dynamic electron correlation than the PT2 level, especially when involving electron detachments from the oxygen atoms.[47] Quantitative assignments of the PE spectra of UO_2^- demands a thorough investigation of the convergence of the calculations with respect to active space and dynamic electron correlations. Such calculations are beyond the computing capability and the scope of the current work.

C. Extensive two-electron transitions and strong electron correlation effects

Table II shows that the main electron configuration for the 1_u and 2_u states is $2\sigma_g^1 1\delta_u^1$ ($^3\Delta_u$), which cannot be accessed from the ground-state configuration ($2\sigma_g^2 1\phi_u^1$) via one-electron transitions, as shown in Eqs. (1)–(3). However, they can be accessed through two-electron transitions, i.e., the detachment of a $2\sigma_g$ electron and at the same time the $1\phi_u$ electron is excited to the $1\delta_u$ orbital. These so-called shakeup processes are direct reflections of strong electron correlation effects. The observation of shakeup processes is a direct result of the multi-configurational nature and SO coupling in the ground state of UO_2^-, which contains a mixing of 12% $^2\Delta_u$ ($2\sigma_g^2 1\delta_u^1$) character (Table III). In fact, except for the bands X and A, which correspond to $^3\Phi_{2u,3u}$ derived by one-electron transitions (Eq. (1)), all the other weak features observed between 1.5 and 5.3 eV are due to two-electron transitions, including the low-lying band *a*, which is assigned to the 4_g state. Our calculations reveal 62 such two-electron excited states up to a binding energy of 3.9 eV, which are compared

with the experimental observation in Table II. All these states can be considered to be derived from one-electron detachment from one of the $2\sigma_g^2 1\phi_u^1$ orbitals with another electron simultaneously excited to a higher-lying unoccupied 5*f*, 6*d*, or 7*p* orbitals (Fig. 2 and Table II), thus making all the $U(5f^2)$, $U(6d^1 5f^1)$ and $U(7p^1 5f^1)$ electronic configurations accessible. The SR CASPT2 calculation results are shown in Table II. The SOC calculations on the excited states including these electron configurations can qualitatively account for all the observed weak features in the PE spectra, as shown in Table II. We note that the assignments of these weak features are semi-quantitative because of the extremely high density of states and the limitation of the accuracy of the approximate quantum mechanical and relativistic methods, as well as unsaturated atomic basis sets used for such a complicated system.

IV. CONCLUDING REMARKS

PES is the most powerful experimental technique to probe electron correlation effects in many-electron systems via the observation of shakeup transitions.[45] However, such clear and numerous shakeup peaks observed for UO_2^- in the valence range are unprecedented. This complexity happens because of the high density of the unoccupied and accessible valence orbitals (5*f*, 6*d*, and 7*p*). The strong electron correlation effects break down the one-electron MO picture and give rise to new excited states that would be difficult to be accessed in any other experiment. The strong electron correlations and spin-orbit couplings produce orders-of-magnitude more photodetachment transitions for UO_2^- than expected on the basis of the Koopmans' theorem. These experimental observations provide new features for the calibration of theoretical methods for actinide systems. The current PES data for UO_2^- provide both a challenge and an opportunity for various WFT and DFT methods aimed at treating molecular systems with strong electron correlation.

ACKNOWLEDGMENTS

The authors wish to thank Dr. C. Romanescu for earlier experimental assistance. The experimental work was funded by the Division of Chemical Sciences, Geosciences, and Biosciences, Office of Basics Energy Sciences of the U.S. Department of Energy through Grant No. DE-FG02-11ER16261 (W. L. Li, T. Jian, G. V. Lopez, and L.-S. Wang) and the theoretical work was supported by NSFC (Grant Nos. 20933003, 91026003, and 21201106) of China (J. Su and J. Li) and the Strategic Priority Research Program (Grant No. XDA02040104) of the Chinese Academy of Sciences (J. Su).

[1] L. R. Morss, N. M. Edelstein, and J. Fuger, *The Chemistry of the Actinide and Transactinide Elements* (Springer, Dordrecht, Netherlands, 2006), Vol. 1.
[2] S. D. Gabelnick, G. T. Reedy, and M. G. Chasanov, J. Chem. Phys. **58**, 4468 (1973).
[3] R. D. Hunt and L. Andrews, J. Chem. Phys. **98**, 3690 (1993).
[4] M. F. Zhou, L. Andrews, N. Ismail, and C. Marsden, J. Phys. Chem. A **104**, 5495 (2000).
[5] L. Gagliardi, B. O. Roos, P. A. Malmqvist, and J. M. Dyke, J. Phys. Chem. A **105**, 10602 (2001).
[6] Q. Chang, Master of Science thesis, The Ohio State University, 2002.
[7] J. D. Han, L. A. Kaledin, V. Goncharov, A. V. Komissarov, and M. C. Heaven, J. Am. Chem. Soc. **125**, 7176 (2003).
[8] J. D. Han, V. Goncharov, L. A. Kaledin, A. V. Komissarov, and M. C. Heaven, J. Chem. Phys. **120**, 5155 (2004).
[9] C. J. Lue, J. Jin, M. J. Ortiz, J. C. Rienstra-Kiracofe, and M. C. Heaven, J. Am. Chem. Soc. **126**, 1812 (2004).
[10] J. Li, B. E. Bursten, L. Andrews, and C. J. Marsden, J. Am. Chem. Soc. **126**, 3424 (2004).
[11] C. Clavaguera-Sarrio, V. Vallet, D. Maynau, and C. J. Marsden, J. Chem. Phys. **121**, 5312 (2004).
[12] L. Gagliardi, M. C. Heaven, J. W. Krogh, and B. O. Roos, J. Am. Chem. Soc. **127**, 86 (2005).
[13] T. Fleig, H. J. A. Jensen, J. Olsen, and L. Visscher, J. Chem. Phys. **124**, 104106 (2006).
[14] I. Infante, E. Eliav, M. J. Vilkas, Y. Ishikawa, U. Kaldor, and L. Visscher, J. Chem. Phys. **127**, 124308 (2007).
[15] J. M. Merritt, J. Han, and M. C. Heaven, J. Chem. Phys. **128**, 084304 (2008).
[16] I. Infante, L. Andrews, X. F. Wang, and L. Gagliardi, Chem.-Eur. J. **16**, 12804 (2010).
[17] M. Pepper and B. E. Bursten, Chem. Rev. **91**, 719 (1991).
[18] J. Marcalo, M. Santos, A. P. de Matos, and J. K. Gibson, Inorg. Chem. **48**, 5055 (2009).
[19] M. D. Michelini, J. Marcalo, N. Russo, and J. K. Gibson, Inorg. Chem. **49**, 3836 (2010).
[20] L. S. Wang, H. S. Cheng, and J. W. Fan, J. Chem. Phys. **102**, 9480 (1995).
[21] J. Akola, M. Manninen, H. Hakkinen, U. Landman, X. Li, and L. S. Wang, Phys. Rev. B **60**, R11297 (1999).
[22] W. Huang and L. S. Wang, Phys. Rev. Lett. **102**, 153401 (2009).
[23] J. P. Perdew, K. Burke, and M. Ernzerhof, Phys. Rev. Lett. **77**, 3865 (1996).
[24] ADF2010.02, SCM, Vrije Universiteit, Amsterdam, see http://www.scm.com.
[25] C. F. Guerra, J. G. Snijders, G. te Velde, and E. J. Baerends, Theor. Chem. Acc. **99**, 391 (1998).
[26] G. te Velde, F. M. Bickelhaupt, E. J. Baerends, C. F. Guerra, S. J. A. Van Gisbergen, J. G. Snijders, and T. J. Ziegler, Comput. Chem. **22**, 931 (2001).
[27] E. van Lenthe and E. J. Baerends, J. Comput. Chem. **24**, 1142 (2003).
[28] E. van Lenthe, E. J. Baerends, and J. G. Snijders, J. Chem. Phys. **99**, 4597 (1993).
[29] H. J. Werner, P. J. Knowles, G. Knizia, F. R. Manby, M. Schütz *et al.*, MOLPRO, version 2012.1, a package of *ab initio* programs, 2012, see http://www.molpro.net.
[30] K. Raghavachari, G. W. Trucks, J. A. Pople, and M. Headgordon, Chem. Phys. Lett. **157**, 479 (1989).
[31] K. Andersson, P. A. Malmqvist, and B. O. Roos, J. Chem. Phys. **96**, 1218 (1992).
[32] G. Ghigo, B. O. Roos, and P. A. Malmqvist, Chem. Phys. Lett. **396**, 142 (2004).
[33] P. A. Malmqvist, B. O. Roos, and B. Schimmelpfennig, Chem. Phys. Lett. **357**, 230 (2002).
[34] B. O. Roos and P. A. Malmqvist, Phys. Chem. Chem. Phys. **6**, 2919 (2004).
[35] X. Y. Cao, M. Dolg, and H. Stoll, J. Chem. Phys. **118**, 487 (2003).
[36] X. Y. Cao and M. Dolg, J. Mol. Struct.: THEOCHEM **673**, 203 (2004).
[37] See http://www.theochem.uni-stuttgart.de/pseudopotentials for the pseudopotentials and basis sets.
[38] R. A. Kendall, T. H. Dunning, and R. J. Harrison, J. Chem. Phys. **96**, 6796 (1992).
[39] M. Dolg and X. Cao, J. Phys. Chem. A **113**, 12573 (2009).
[40] R. G. Denning, Struct. Bond **79**, 215 (1992).
[41] R. G. Denning, J. Phys. Chem. A **111**, 4125 (2007).
[42] S. P. Mcglynn and J. K. Smith, J. Mol. Spectrosc. **6**, 164 (1961).
[43] M. V. Ryzhkov and V. A. Gubanov, J. Radioanal. Nucl. Chem. **143**, 85 (1990).
[44] J. Su, K. Zhang, W. H. E. Schwarz, and J. Li, Inorg. Chem. **50**, 2082 (2011).
[45] S. Suzer, S. T. Lee, and D. A. Shirley, Phys. Rev. A **13**, 1842 (1976).
[46] J. Su, Y. L. Wang, F. Wei, W. H. E. Schwarz, and J. Li, J. Chem. Theory Comput. **7**, 3293 (2011).
[47] Y. Li, J. Su, E. Mitchell, G. Zhang, and J. Li, Sci. China Chem. **56**, 1671 (2013).